Experimental verification of the origin of positive linear magnetoresistance in $CoFe(V_{1-x}Mn_x)Si$ Heusler alloys

S. Yamada,[1,2,*] S. Kobayashi,[2] A. Masago,[1] L. S. R. Kumara,[3] H. Tajiri,[3] T. Fukushima,[4,1] S. Abo,[5] Y. Sakuraba,[6] K. Hono,[6] T. Oguchi,[7,1,8] and K. Hamaya[1,2,†]

[1]*Center for Spintronics Research Network, Graduate School of Engineering Science, Osaka University, Toyonaka, Osaka 560-8531, Japan*
[2]*Department of Systems Innovation, Graduate School of Engineering Science, Osaka University, Toyonaka, Osaka 560-8531, Japan*
[3]*Japan Synchrotron Radiation Research Institute, Sayo, Hyogo 679-5198, Japan*
[4]*Institute for Datability Science, Osaka University, Suita, Osaka 565-0871 Japan*
[5]*Center for Science and Technology under Extreme Conditions, Graduate School of Engineering Science, Osaka University, Toyonaka, Osaka 560-8531, Japan*
[6]*Research Center for Magnetic and Spintronic Materials, National Institute for Materials Science, Tsukuba, Ibaraki 305-0047, Japan*
[7]*Institute of Scientific and Industrial Research, Osaka University, Ibaraki, Osaka 567-0047, Japan*
[8]*MaDIS, National Institute for Materials Science, Tsukuba, Ibaraki 305-0047, Japan*

(Received 12 June 2019; revised manuscript received 27 September 2019; published 25 November 2019)

The origin of the positive linear magnetoresistance (PLMR) effect at low temperatures in $CoFe(V_{1-x}Mn_x)Si$ Heusler alloys is discussed. From anomalous dispersion x-ray diffraction measurements, we can clarify that the crystal structure of the epitaxial CoFeVSi films grown by molecular beam epitaxy (MBE) is $L2_1B$ type. By employing the substitution of Mn for V in the CoFeVSi film in MBE conditions, we experimentally demonstrate homogeneous $CoFe(V_{1-x}Mn_x)Si$ films and systematic control of the magnetic moments. The PLMR effect gradually decreases with increasing Mn contents but it can be seen even for $CoFe(V_{0.5}Mn_{0.5})Si$. We note that the PLMR effect disappears for $CoFe(V_{0.25}Mn_{0.75})Si$. According to theoretical calculations of the electronic band structures of $CoFe(V_{1-x}Mn_x)Si$, the gaplesslike electronic band structure due to the V-*d* state in the minority spins of CoFeVSi is varied to the band gap by increasing the substitution of Mn. This means that the electronic band structure near the Fermi level in $CoFe(V_{1-x}Mn_x)Si$ can be experimentally controlled by substituting Mn for V. From these considerations, we can conclude that the PLMR effect in $CoFe(V_{1-x}Mn_x)Si$ is caused by the presence of the V state-induced gaplesslike structure in the minority spin electronic band near the Fermi level.

DOI: 10.1103/PhysRevB.100.195137

I. INTRODUCTION

Magnetoresistance (MR) effect has been studied in various fields of condensed matter physics over the years. Because of the Lorentz force, the scattering of charge carriers in nonmagnetic materials is generally enhanced with increasing external magnetic fields (H), leading to the increase in the resistance. The resistance change in nonmagnetic materials is proportional to the square of H [1], resulting in the parabolic increase in the resistance with increasing H. This feature is a positive MR effect in nonmagnetic materials such as semiconductors. In ferromagnetic materials, on the other hand, since the spin-polarized carriers are strongly coupled with the local magnetic moments, the ordering of magnetic moments in ferromagnetic materials can affect the carrier scattering. That is, if the fluctuation of the magnetization in ferromagnetic materials was suppressed by applying H, the spin-related carrier scattering can also be suppressed [2,3], leading to the decrease in the resistance. This is a conventional negative MR effect in ferromagnetic materials. In addition to this, positive or negative resistance changes derived from the anisotropic magnetoresistance (AMR) effect, in which the resistance depends on the relative orientation between the current flow and the magnetization direction, can constantly be observed [4,5].

Even for ferromagnetic materials with a high Curie temperature (T_C), positive linear magnetoresistance (PLMR) effect was recently observed at low temperatures for some of ferromagnetic Heusler alloys such as Mn_2CoAl [6] and Fe_2CoSi [7]. The Heusler alloys having a *XA*-type crystal structure, Mn_2CoAl and Fe_2CoSi, are predicted as a spin-gapless semiconductor (SGS) [8] and a zero-gap half-metal, respectively. For both Mn_2CoAl [6] and Fe_2CoSi [7], a crossover from the PLMR effect to the conventional negative MR one can be observed with increasing external temperature. In the meanwhile, the PLMR effect has been reported in various gapless materials [6–13]. One of the possible origins of the PLMR effect is due to the quantum linear MR effect [14] depending on the electronic band structure with gapless linear dispersion [6–13]. In particular, it was experimentally shown that the appearance of the PLMR effect is strongly related to the gapless electronic band structures near the Fermi level, which can be tuned by applying hydrostatic pressure, for silver chalcogenides such as $Ag_{2\pm\delta}Te$ having

*yamada@ee.es.osaka-u.ac.jp
†hamaya@ee.es.osaka-u.ac.jp

a semimetallic electronic band structure [10]. Very recently, we also observed the PLMR effect at low temperatures in an equiatomic quaternary Heusler alloy CoFeVSi [15], in which the calculated density of states (DOS) of CoFeVSi is not a clear SGS-like electronic band structure. In the detailed investigation of magnetotransport properties and theoretical calculations of electronic band structures [15], we tentatively speculated that the charge carriers at low temperatures in CoFeVSi were dominated by a specific gaplesslike electronic band structure related to the V-*d* state, resulting in the PLMR effect. However, for these Heusler-alloy systems including Mn_2CoAl [6] and Fe_2CoSi [7], experimental evidence for the origin of the PLMR effect has not been obtained yet.

In this article we experimentally address the origin of the PLMR effect in $CoFe(V_{1-x}Mn_x)Si$. From the detailed structural analyses, most of the epitaxial CoFeVSi films consist of the $L2_1$B-type crystal structure. By employing the substitution of Mn for V in the CoFeVSi film in molecular beam epitaxy conditions, the lattice constant can systematically be changed by following Vegard's law. For the epitaxial $CoFe(V_{0.25}Mn_{0.75})Si$ film, we can observe homogeneous microstructures and each element. In addition, magnetic properties are systematically tuned with changing the Mn contents, consistent with theoretical expectation. Note that the PLMR effect is gradually decreased with increasing Mn contents and it disappears for the epitaxial $CoFe(V_{0.25}Mn_{0.75})Si$ film. According to theoretical calculations of the electronic band structures of $CoFe(V_{0.25}Mn_{0.75})Si$, the gaplesslike electronic band structure due to the V-*d* state in the minority spins of CoFeVSi was varied to the band gap by increasing the substitution of Mn. This means that the electronic band structure near the Fermi level in $CoFe(V_{1-x}Mn_x)Si$ can be experimentally controlled by substituting Mn for V. From these considerations, we can conclude that the PLMR effect in $CoFe(V_{1-x}Mn_x)Si$ is caused by the presence of the V state-induced gapless structure in the minority spin electronic band near E_F.

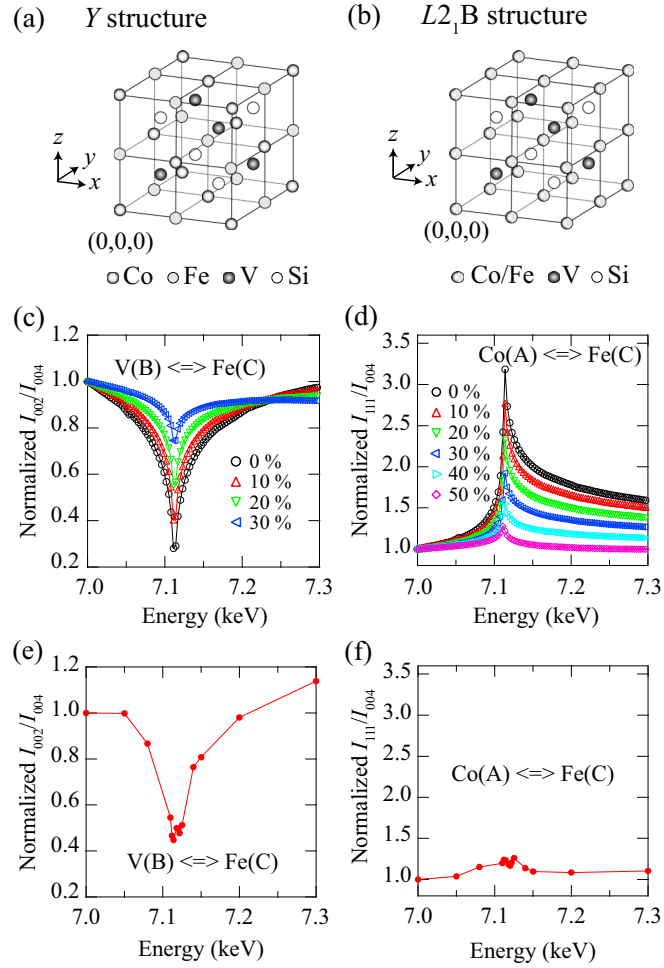

FIG. 1. Crystal structures for (a) *Y*-type and (b) $L2_1$B-type CoFeVSi. Calculated x-ray energy dependence of (c) I_{002}/I_{004} with V-Fe disorder and (d) I_{111}/I_{004} with Co-Fe disorder near the Fe-*K* absorption edge. I_{002}/I_{004} and I_{111}/I_{004} are normalized by the value at $E = 7.0$ keV. Experimentally measured (e) I_{002}/I_{004} and (f) I_{111}/I_{004} versus E for epitaxial CoFeVSi films near the Fe-*K* absorption edge.

II. SAMPLES AND STRUCTURES

Prior to the sample fabrication and characterizations, we briefly explain the crystal structure of CoFeVSi, where there are two types, *Y* type [Fig. 1(a)] and $L2_1$B type [Fig. 1(b)]. For the *Y*-type structure, there are four different crystal sites denoted as A(0,0,0), B($\frac{1}{4}$, $\frac{1}{4}$, $\frac{1}{4}$), C($\frac{1}{2}$, $\frac{1}{2}$, $\frac{1}{2}$), and D($\frac{3}{4}$, $\frac{3}{4}$, $\frac{3}{4}$) in Wyckoff coordinates and Co, V, Fe, and Si occupy the A, B, C, and D sites, respectively. When Co-Fe disorder occurs, the crystal structure is defined as the $L2_1$B structure. Because the atomic scattering factors between Co and Fe are close to each other at the Cu $K\alpha$ energy, it is difficult to distinguish between the *Y*- or $L2_1$B-type structure in conventional XRD measurements.

In this paper, CoFeVSi films with a thickness of ~10 nm were grown on $MgAl_2O_4(100)$ substrates at 300 °C by a nonstoichiometric molecular beam epitaxy (MBE) technique [15–20], where the mismatch between the lattice constant of CoFeVSi (0.5642 nm) [15] and half of the diagonal length of $MgAl_2O_4$ ($0.8083 \times 1/\sqrt{2} = 0.5715$ nm) is ~1.3%. The detailed growth procedure is shown in our previous work [15]. *In situ* reflection high-energy electron diffraction (RHEED) observations during the growth of CoFeVSi layer clearly exhibited symmetrical streaks, showing good two-dimensional epitaxial growth. The quality of the CoFeVSi films was almost the same as shown in our previous work [15].

To distinguish whether the *Y*- or $L2_1$B-type structure was formed, we performed anomalous dispersion XRD (AXRD) measurements [21–23]. Before the measurements, we calculated x-ray energy (E) dependence of integrated intensities of 004 (I_{004}), 002 (I_{002}), and 111 (I_{111}) reflections from 7.0 to 7.3 keV around Fe-*K* absorption edge (7.11 keV) for the different Co-Fe and Fe-V disordered levels. Figures 1(c) and 1(d) show the calculated values of I_{002}/I_{004} with V-Fe disorder and I_{111}/I_{004} with Co-Fe disorder near the Fe-*K* absorption edge, respectively, where I_{002}/I_{004} and I_{111}/I_{004} are normalized by the value at $E = 7.0$ keV. From these calculations, the value of I_{002}/I_{004} ($E = 7.1$ keV) gradually increases with increasing the Fe-V disorder, while that of I_{111}/I_{004} gradually decreases with increasing the Co-Fe disorder. Note that the calculated value of I_{004} was insensitive to the Fe-V and Co-Fe disorder at the Fe-*K* absorption edge. For the grown epitaxial CoFeVSi

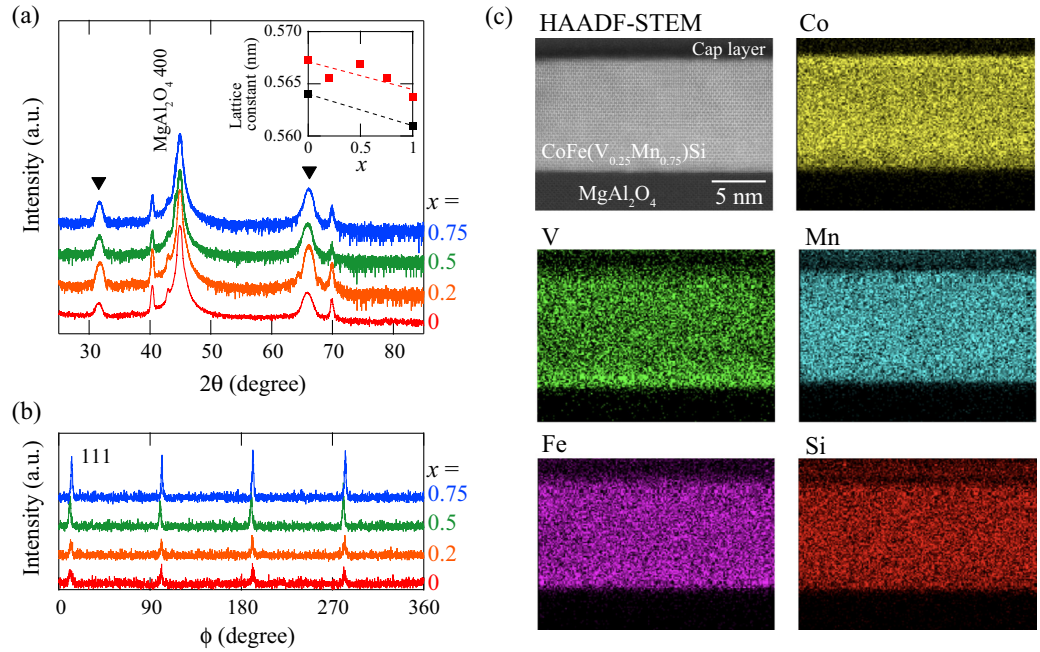

FIG. 2. (a) θ-2θ XRD patterns of the CoFe($V_{1-x}Mn_x$)Si films for various x. Inverted closed triangles represent 200 and 400 diffraction peaks of CoFe($V_{1-x}Mn_x$)Si. The inset shows the lattice constant of the epitaxial CoFe($V_{1-x}Mn_x$)Si films estimated from (a) (red), together with the theoretical values (black) [15,27,28]. (b) ϕ-scan measurement of (111) plane of the CoFe($V_{1-x}Mn_x$)Si films. (c) HAADF-STEM image and EDX mapping images for each element in an epitaxial CoFe($V_{0.25}Mn_{0.75}$)Si film.

films, we performed the AXRD measurements of I_{004}, I_{002}, and I_{111} for various E near the Fe-K absorption edge at the beamline BL13XU in SPring-8 [24,25]. Figures 1(e) and 1(f) display the experimentally measured I_{002}/I_{004} and I_{111}/I_{004}, respectively, where I_{002}/I_{004} and I_{111}/I_{004} are also normalized by the value at $E = 7.0$ keV. By comparing the experimental results with the calculated ones, we can recognize that the degree of the V-Fe disorder is less than 10%, whereas that of the Co-Fe disorder is nearly 50%. As a result, we regard the crystal structure of the epitaxial CoFeVSi films as $L2_1$B-type.

Because Mn atoms preferentially occupy the B site in the Heusler alloy [16,26], Mn can be ideally substituted for V in CoFeVSi, leading to CoFe($V_{1-x}Mn_x$)Si. Thus, by employing MBE techniques, we also conducted the growth of Mn-substituted CoFeVSi films on $MgAl_2O_4$(100) substrates and good two-dimensional epitaxial growth was demonstrated in all the films with $x = 0.2$, 0.5, and 0.75. Figure 2(a) shows θ-2θ XRD patterns of the epitaxial CoFe($V_{1-x}Mn_x$)Si films for various x. The 200 and 400 diffraction peaks of CoFe($V_{1-x}Mn_x$)Si are observed at 2θ of $\sim$31.5° and $\sim$65.8° (inverted closed triangles), respectively, indicating the formation of (100)-oriented epitaxial films. The estimated lattice constants (red) from the XRD data in Fig. 2(a), together with the theoretical values (black) [15,27,28], are shown in the inset of Fig. 2(a). Although there is a slight difference in the lattice constants between experiment and theory, the change following Vegard's law can be seen with increasing x. This means that the substitution of Mn for V in CoFeVSi is demonstrated experimentally. The ϕ-scan measurements of (111) plane of CoFe($V_{1-x}Mn_x$)Si films for various x are performed in Fig. 2(b). For all the films, sharp diffraction peaks with fourfold symmetry are seen, indicating the formation of Y- or $L2_1$B-type structures in the CoFe($V_{1-x}Mn_x$)Si films. According to a theoretical work [28], CoFeMnSi with a $L2_1$B-type structure is also energetically stable. Considering the theoretical work [28] and Fig. 2, we speculate that the epitaxial CoFe($V_{1-x}Mn_x$)Si films consist of the $L2_1$B-type structure.

For CoFe($V_{1-x}Mn_x$)Si films, further structural investigations were carried out by cross-sectional high-angle annular dark-field scanning transmission electron microscopy (HAADF-STEM) and energy dispersive x-ray spectroscopy (EDX). Figure 2(c) shows an enlarged HAADF-STEM image and EDX mapping images for each element of an epitaxial CoFe($V_{0.25}Mn_{0.75}$)Si film. Since the contrast of the HAADF-STEM image is nearly homogeneous over the measured area, we can judge that the epitaxial CoFe($V_{0.25}Mn_{0.75}$)Si film on $MgAl_2O_4$(100) is uniformly grown, similar to the non-substituted CoFeVSi films previously shown in Ref. [15]. From the EDX mapping images, the atomic composition fluctuation in the constituent elements cannot be seen. These results mean the absence of phase separation in the epitaxial CoFe($V_{0.25}Mn_{0.75}$)Si film. Although there is no experimental report of bulk CoFeVSi with Mn substitution, we can clearly demonstrate the Mn substituted CoFeVSi films.

III. MAGNETIC AND ELECTRICAL PROPERTIES

We also characterized magnetic properties of the epitaxial CoFe($V_{1-x}Mn_x$)Si films. Figure 3(a) shows the saturation magnetic moment (M_S) versus x at 10 K (blue), together with the calculated values for $L2_1$B-type CoFe($V_{1-x}Mn_x$)Si (red) and reported ones (black) [27–29]. Here the theoretically calculated values of M_S for $L2_1$B-type CoFeVSi and CoFeMnSi are 1.7 and 4.0 μ_B/f.u., respectively. In theory, the value of M_S can be systematically controlled by increasing x.

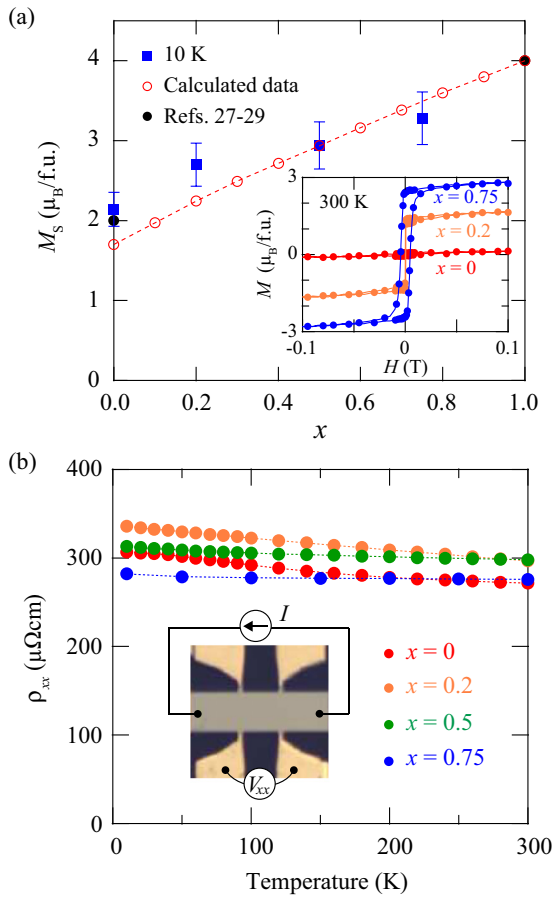

FIG. 3. (a) M_S versus x for CoFe($V_{1-x}Mn_x$)Si films at 10 K (blue), with the calculated values (red) and reported ones (black) [27–29]. The inset shows M-H curve at 300 K for $x = 0$, 0.2 and 0.75. (b) Temperature dependence of ρ_{xx} for the epitaxial CoFe($V_{1-x}Mn_x$)Si films. The inset shows a fabricated Hall-bar device for transport measurements.

The experimental data also varies systematically, implying that the substitution of Mn for V in CoFeVSi is successful. The inset of Fig. 3(a) shows the magnetization (M-H) curves of the CoFe($V_{1-x}Mn_x$)Si films at 300 K for $x = 0$, 0.2, and 0.75. Reflecting the difference in T_C between CoFeVSi (∼271 K) [15] and CoFeMnSi (∼623 K) [27,29], we can clearly see that hysteresis behavior appears with increasing x at 300 K. From these structural and magnetic properties, we have experimentally verified that the substitution of Mn for V in CoFeVSi is successfully carried out by employing the MBE technique.

To measure electrical and magnetotransport properties, the CoFe($V_{1-x}Mn_x$)Si films were patterned into Hall-bar devices with 80 × 80 μm^2 in size, as shown in the inset of Fig. 3(b), by conventional photolithography and Ar ion milling. The longitudinal resistance ($R_{xx} = V_{xx}/I$) was recorded by a standard DC four-terminal method and electrical resistivity (ρ_{xx}) can be estimated from the recorded value of R_{xx}. Figure 3(b) shows temperature dependence of ρ_{xx} for various x. All the ρ_{xx}-T curves exhibit nearly temperature-independent behavior. In the previous studies of Heusler alloys with SGS-like or semimetal-like electronic band structures, small temperature dependence or temperature independence of ρ_{xx} has already been reported [6,19,29]. Thus, these ρ_{xx}-T features indicate the presence of SGS-like or semimetal-like electronic band structures in the epitaxial CoFe($V_{1-x}Mn_x$)Si films.

IV. MAGNETORESISTANCE PROPERTIES

To examine the correlation between the PLMR effect in CoFeVSi and the substitution of Mn for V, we performed magnetotransport measurements of the epitaxial CoFe($V_{1-x}Mn_x$)Si films for various x. Field-dependent MR ratio at various temperatures is shown in Figs. 4(a)–4(d), where the MR ratio is defined as $[R_{xx}(H) - R_{xx}(0)]/R_{xx}(0) \times 100\%$, and $R_{xx}(H)$ and $R_{xx}(0)$ are the electrical resistance with and without applying H, respectively. In the measurements, H was applied in the film plane parallel to the current direction, as shown in the inset of Fig. 4(a), to avoid superimposing the influence of the AMR effect and/or the anomalous Hall effect in the measurement data. As described in our previous study on $x = 0$ (CoFeVSi) [15], the PLMR effect appears below 200 K despite the ferromagnetic nature in Fig. 4(a). It should be noted that the PLMR effect can be observed even for $x = 0.5$ [Fig. 4(c)] although the magnitude becomes gradually smaller with increasing x. When $x = 0.75$ [Fig. 4(d)], the PLMR effect disappears even at low temperature. The above features could also be reproduced in the data for applying H perpendicular to the film plane (not shown here) despite superimposing the influence of the AMR effect and/or the anomalous Hall effect.

From Hall-effect measurements for the CoFe($V_{1-x}Mn_x$)Si films, we also observed a crossover of the dominant conduction carriers from holes to electrons with decreasing temperature for $x \leqslant 0.5$ while the dominant conduction carriers were electrons at all the measurement temperatures for $x = 0.75$ (not shown here). We note that the crossover of the dominant conduction carriers is caused by the SGS-like or semimetal-like electronic band structures for $x \leqslant 0.5$, in which the conduction and valence band edges touch or cross at around the Fermi level. This is also a large difference in the magnetotransport properties between CoFe($V_{0.5}Mn_{0.5}$)Si and CoFe($V_{0.25}Mn_{0.75}$)Si. Because the reliable substitution of Mn for V in CoFeVSi can be considered in Figs. 2 and 3(a), we can interpret that the change in the PLMR effect with increasing x is attributed to the change in the electronic band structure at around E_F [15].

V. ELECTRONIC BAND STRUCTURE

To further discuss the electronic band structure in CoFe($V_{1-x}Mn_x$)Si in detail, we performed first-principles density-functional theory calculations using the Akai-KKR package [30]. The package is based on the Korringa-Kohn-Rostoker (KKR) method with a coherent potential approximation (CPA), and the following conditions were assumed [31–33]. The Perdew-Burke-Ernzerhof (PBE) potential was used for the exchange-correlation calculations. The k-sampling points were 1000. The lattice constant was fixed to the experimental value of 0.5677 nm. Figure 5 displays spin-resolved Bloch spectral functions and density of states (DOS) of CoFe($V_{0.25}Mn_{0.75}$)Si that possesses the $L2_1$B-type structure [15,29]. The spectral function resembles the band

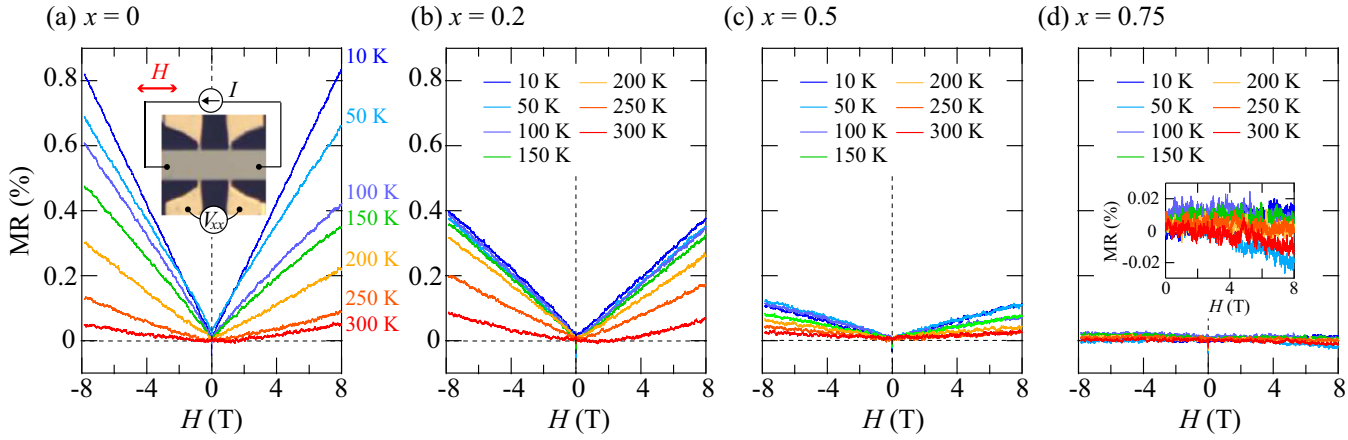

FIG. 4. Field-dependent MR ratio at various temperatures for the epitaxial CoFe($V_{1-x}Mn_x$)Si films, where the magnetic field was applied in the film plane parallel to the current direction.

structures of Y-type and $L2_1$B-type CoFeVSi [15]. The band structures of CoFe($V_{0.25}Mn_{0.75}$)Si are smeared out by the Co-Fe disorder in the Heusler alloy, because the wave vectors are not a good quantum number [34]. The disordered Co-Fe states around the Fermi level (E_F) occupied most of the majority spin states, leading to no noteworthy variation in the majority spin bands by increasing x. On the other hand, we note that a remarkable band gap appears at around the X point in the minority spins. This feature is different from that for CoFeVSi [15], in which the top of the valence band at around X point below E_F touches the bottom of the conduction band, i.e., a gaplesslike band structure. From the minority spin distribution of DOS in Fig. 5, the electron pocket located at around the X point in the minority spin contribution mainly consists of the V-d states. This character basically provides the same mechanism as the relation between Y-type and $L2_1$B-type CoFeVSi [15]. Moreover, it was theoretically predicted that the V-d bands at around X point in the minority spins are gradually pushed down toward energetically lower region when the substitution of Mn for V in CoFeVSi is decreased [35]. This means that the gaplesslike structure in the minority spin electronic band near E_F in CoFeVSi can be varied to a clear band gap by substituting Mn for V, which is consistent with the half-metallic behavior of epitaxial CoFeMnSi films [36]. Since the PLMR effect gradually decreases with substituting Mn for V in CoFe($V_{1-x}Mn_x$)Si in Fig. 4, this feature is strongly related to the variation in the minority spin electronic band structure dominated by the V-d states. From these considerations, a direct evidence for the PLMR effect due to the presence of the V state-induced gaplesslike structure in the minority spin electronic band near E_F, discussed in our previous study [15], is experimentally presented.

Finally we comment on the presence of the PLMR effect in CoFe($V_{1-x}Mn_x$)Si. As described in this paper, we experimentally found that the PLMR effect in the CoFe($V_{1-x}Mn_x$)Si films originates from the V-d states in the minority spin electronic band near E_F. Up to now, similar PLMR effects have been observed for Mn_2CoAl [6] and Fe_2CoSi [7], where it was expected that both materials have gapless electronic band structures near E_F. Considering these phenomena in Heusler alloys, we can also recognize that the observed PLMR effect is surely due to the quantum linear MR effect [14] depending on the electronic band structure with gapless linear dispersion, as discussed in Refs. [6,7].

VI. CONCLUSION

We experimentally studied the origin of the PLMR effect in CoFe($V_{1-x}Mn_x$)Si Heusler alloys. From AXRD measurements, we clarified that the crystal structure of the epitaxial CoFeVSi films grown by MBE is $L2_1$B type. By employing the substitution of Mn for V in the CoFeVSi film in MBE conditions, we experimentally demonstrated homogeneous CoFe($V_{1-x}Mn_x$)Si films and systematic control

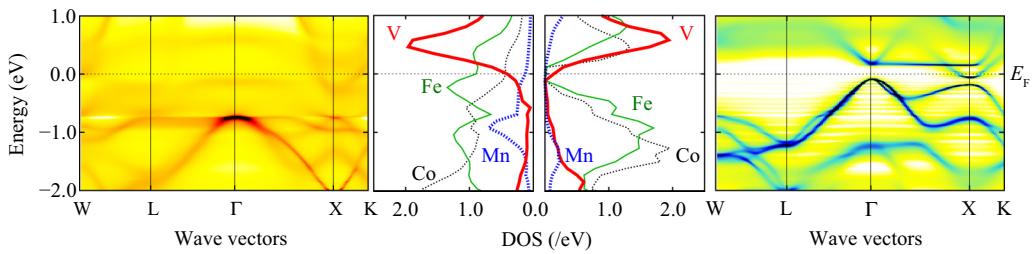

FIG. 5. Electronic structures of $L2_1$B-type CoFe($V_{0.25}Mn_{0.75}$)Si. Ends and central two figures display Bloch spectral functions and density of states, respectively, where the left and right sides indicate electronic structures of the majority and minority spin states, respectively. In the density of states, red solid, blue dashed, green solid, and black dashed lines are V, Mn, Fe, and Co states, respectively.

of the magnetic moments. The PLMR effect gradually decreased with increasing Mn contents but it was observed even for $CoFe(V_{0.5}Mn_{0.5})Si$. It should be noted that the PLMR effect disappeared for $CoFe(V_{0.25}Mn_{0.75})Si$. According to theoretical calculations of the electronic band structures of $CoFe(V_{1-x}Mn_x)Si$, the gaplesslike electronic band structure due to the V-*d* state in the minority spins of CoFeVSi was varied to the band gap by increasing the substitution of Mn. That means that the electronic band structure near the Fermi level in $CoFe(V_{1-x}Mn_x)Si$ can be experimentally controlled by substituting Mn for V. From these considerations, we can conclude that the PLMR effect in $CoFe(V_{1-x}Mn_x)Si$ is caused by the presence of the V state-induced gaplesslike structure in the minority spin electronic band near E_F.

ACKNOWLEDGMENTS

This work was partly supported by JSPS KAKENHI (Grants No. 16H02333, No. 17H06152, No. 18KK0111, and No. 19H05616). The synchrotron radiation experiments were performed on beamline BL13XU at SPring-8 with the approval of the Japan Synchrotron Radiation Research Institute (JASRI) (Proposals No. 2018A1016, No. 2018A2052, and No. 2018A0927).

[1] J.-P. Jan, Solid State Phys. **5**, 1 (1957).
[2] R. von Helmolt, J. Wecker, B. Holzapfel, L. Schultz, and K. Samwer, Phys. Rev. Lett. **71**, 2331 (1993).
[3] F. Matsukura, H. Ohno, A. Shen, and Y. Sugawara, Phys. Rev. B **57**, R2037(R) (1998).
[4] I. A. Campbell, A. Fert, and O. Jaoul, J. Phys. C: Solid State Phys. **3**, S95 (1970).
[5] T. McGuire and R. Potter, IEEE Trans. Magn. **11**, 1018 (1975).
[6] S. Ouardi, G. H. Fecher, C. Felser, and J. Kübler, Phys. Rev. Lett. **110**, 100401 (2013).
[7] Y. Du, G. Z. Xu, X. M. Zhang, Z. Y. Liu, S. Y. Yu, E. K. Liu, W. H. Wang, and G. H. Wu, Europhys. Lett. **103**, 37011 (2013).
[8] X. L. Wang, Phys. Rev. Lett. **100**, 156404 (2008); X. L. Wang, S. X. Dou, and C. Zhang, NPG Asia Mater. **2**, 31 (2010).
[9] R. Xu, A. Husmann, T. F. Rosenbaum, M.-L. Saboungi, J. E. Enderby, and P. B. Littlewood, Nature (London) **390**, 57 (1997)
[10] M. Lee, T. F. Rosenbaum, M.-L. Saboungi, and H. S. Schnyders, Phys. Rev. Lett. **88**, 066602 (2002).
[11] A. L. Friedman, J. L. Tedesco, P. M. Campbell, J. C. Culbertson, E. Aifer, F. K. Perkins, R. L. Myers-Ward, J. K. Hite, C. R. Eddy Jr., G. G. Jernigan, and D. K. Gaskill, Nano Lett. **10**, 3962 (2010).
[12] T. Liang, Q. Gibson, M. N. Ali, M. Liu, R. J. Cava, and N. P. Ong, Nat. Mater. **14**, 280 (2014).
[13] C. Shekhar, A. K. Nayak, Y. Sun, M. Schmidt, M. Nicklas, I. Leermakers, U. Zeitler, Y. Skourski, J. Wosnitza, Z. Liu, Y. Chen, W. Schnelle, H. Borrmann, Y. Grin, C. Felser, and B. Yan, Nat. Phys. **11**, 645 (2015).
[14] A. A. Abrikosov, Phys. Rev. B **58**, 2788 (1998); Europhys. Lett. **49**, 789 (2000).
[15] S. Yamada, S. Kobayashi, F. Kuroda, K. Kudo, S. Abo, T. Fukushima, T. Oguchi, and K. Hamaya, Phys. Rev. Mater. **2**, 124403 (2018).
[16] K. Hamaya, H. Itoh, O. Nakatsuka, K. Ueda, K. Yamamoto, M. Itakura, T. Taniyama, T. Ono, and M. Miyao, Phys. Rev. Lett. **102**, 137204 (2009).
[17] S. Yamada, K. Tanikawa, S. Oki, M. Kawano, M. Miyao, and K. Hamaya, Appl. Phys. Lett. **105**, 071601 (2014).
[18] Y. Fujita, M. Yamada, M. Tsukahara, T. Oka, S. Yamada, T. Kanashima, K. Sawano, and K. Hamaya, Phys. Rev. Appl. **8**, 014007 (2017).
[19] K. Arima, F. Kuroda, S. Yamada, T. Fukushima, T. Oguchi, and K. Hamaya, Phys. Rev. B **97**, 054427 (2018).
[20] K. Kudo, S. Yamada, J. Chikada, Y. Shimanuki, T. Ishibe, S. Abo, H. Miyazaki, Y. Nishino, Y. Nakamura, and K. Hamaya, Phys. Rev. B **99**, 054201 (2019).
[21] B. Ravel, J. O. Cross, M. P. Raphael, V. G. Harris, R. Ramesh, and V. Saraf, Appl. Phys. Lett. **81**, 2812 (2002).
[22] S. Li, Y. K. Takahashi, Y. Sakuraba, N. Tsuji, H. Tajiri, Y. Miura, J. Chen, T. Furubayashi, and K. Hono, Appl. Phys. Lett. **108**, 122404 (2016).
[23] S. Li, T. Nakatani, K. Masuda, Y. Sakuraba, X. D. Xu, T. T. Sasaki, H. Tajiri, Y. Miura, T. Furubayashi, and K. Hono, Acta Mater. **142**, 49 (2018).
[24] O. Sakata, Y. Furukawa, S. Goto, T. Mochizuki, T. Uruga, K. Takeshita, H. Ohashi, T. Ohata, T. Matsushita, S. Takahashi, H. Tajiri, T. Ishikawa, M. Nakamura, M. Ito, K. Sumitani, T. Takahashi, T. Shimura, A. Saito, and M. Takahasi, Surf. Rev. Lett. **10**, 543 (2003).
[25] H. Tajiri, H. Yamazaki, H. Ohashi, S. Goto, O. Sakata, and T. Ishikawa, J. Synchrotron Radiat. **26**, 750 (2019).
[26] S. Yoon and J. G. Booth, J. Phys. F: Metal Phys. **7**, 1079 (1977).
[27] V. Alijani, S. Ouardi, G. H. Fecher, J. Winterlik, S. S. Naghavi, X. Kozina, G. Stryganyuk, C. Felser, E. Ikenaga, Y. Yamashita, S. Ueda, and K. Kobayashi, Phys. Rev. B **84**, 224416 (2011).
[28] Z. Ren, Y. Zhao, J. Jiao, N. Zheng, H. Liu, and S. Li, J. Supercond. Nov. Magn. **29**, 3181 (2016).
[29] L. Bainsla, A. I. Mallick, M. M. Raja, A. K. Nigam, B. S. D. Ch. S. Varaprasad, Y. K. Takahashi, A. Alam, K. G. Suresh, and K. Hono, Phys. Rev. B **91**, 104408 (2015).
[30] H. Akai, J. Phys. Soc. Jpn. **51**, 468 (1982).
[31] J. Korringa, Physica **13**, 392 (1947); W. Kohn and N. Rostoker, Phys. Rev. **94**, 1111 (1954).
[32] G. M. Stocks, W. M. Temmerman, and B. L. Gyorffy, Phys. Rev. Lett. **41**, 339 (1978).
[33] H. Shiba, Prog. Theor. Phys. **46**, 77 (1971).
[34] H. Ebert, A. Vernes, and J. Banhart, Solid State Commun. **104**, 243 (1997).
[35] See Supplemental Material at http://link.aps.org/supplemental/10.1103/PhysRevB.100.195137 for details of the minority spin electronic structure of $CoFe(V_{1-x}Mn_x)Si$ ($x = 0,\ 0.3,\ 0.7$, and 1.0); changes in the V-*d* band around *X* point and the Fermi level are shown; and in addition, the dependence of the band structure on calculation methods is mentioned, which includes Refs. [37, 38].
[36] L. Bainsla, K. Z. Suzuki, M. Tsujikawa, H. Tsuchiura, M. Shirai, and S. Mizukami, Appl. Phys. Lett. **112**, 052403 (2018).
[37] H. J. F. Jansen and A. J. Freeman, Phys. Rev. B **30**, 561 (1984).
[38] R H. Parmenter, Phys. Rev. **97**, 587 (1955).